BIOCHEMISTRY
including biophysical chemistry & molecular biology

Rapid Report

pubs.acs.org/biochemistry

In Crystallo Capture of a Covalent Intermediate in the UDP-Galactopyranose Mutase Reaction

Ritcha Mehra-Chaudhary,[†] Yumin Dai,[‡] Pablo Sobrado,*[,‡] and John J. Tanner*[,§]

[†]Structural Biology Core, University of Missouri—Columbia, Columbia, Missouri 65211, United States

[‡]Department of Biochemistry and Center for Drug Discovery, Virginia Tech, Blacksburg, Virginia 24061, United States

[§]Departments of Biochemistry and Chemistry, University of Missouri—Columbia, Columbia, Missouri 65211, United States

Supporting Information

ABSTRACT: UDP-galactopyranose mutase (UGM) plays an essential role in galactofuranose biosynthesis in pathogens by catalyzing the conversion of UDP-galactopyranose to UDP-galactofuranose. Here we report the first crystal structure of a covalent intermediate in the UGM reaction. The 2.3 Å resolution structure reveals UDP bound in the active site and galactopyranose linked to the FAD through a covalent bond between the anomeric C of galactopyranose and N5 of the FAD. The structure confirms the role of the flavin as nucleophile and supports the hypothesis that the proton destined for O5 of galactofuranose is shuttled from N5 of the FAD via O4 of the FAD.

UDP-galactopyranose mutase (UGM) catalyzes the interconversion of UDP-galactopyranose (UDP-Gal*p*) and UDP-galactofuranose (UDP-Gal*f*) (Scheme 1). The latter sugar nucleotide is the donor substrate for enzymes that incorporate Gal*f* into myriad biomolecules that form the host−pathogen barriers in bacteria, fungi, protozoan parasites, and nematodes.[1] Because Gal*f* has never been found in animals, the inhibition of Gal*f* biosynthesis is a potential drug design strategy.

Scheme 1. Reaction Catalyzed by UGM

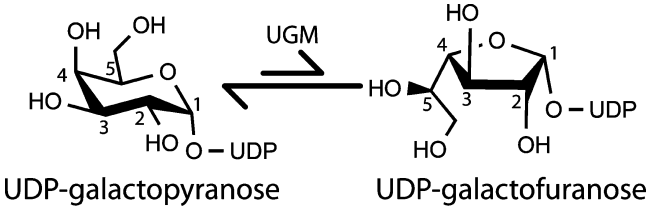

Gal*f* originates in the UGM reaction, which suggests that UGM is a good drug target. Indeed, UGM is an essential enzyme in *Mycobacterium tuberculosis*[2,3] and a virulence factor in eukaryotic pathogens, including the fungus *Aspergillus fumigatus* (causative agent of aspergillosis) and the trypanosomal parasite *Leishmania* spp.[4,5] Also, Gal*f*-containing glycoconjugates are involved in the mechanism of myocardial damage by *Trypanosoma cruzi*, the causative agent of Chagas disease.[6] Furthermore, Gal*f* has been identified in nematodes,[7−9] suggesting that UGMs from *Brugia malayi* (causing elephantiasis) and *Onchocerca volvulus* (river blindness) are potential targets.

UGM also is important to basic science as the prototype of noncanonical flavoenzymes. Unlike traditional flavoenzymes, the redox state of the flavin in UGM is unchanged during the catalytic cycle. Rather, the FAD coenzyme in UGM functions as a nucleophile that attacks the anomeric C atom of the substrate (C1). This role requires that the flavin be in the reduced state for activity (Scheme 2a). The accepted mechanism begins with nucleophilic attack of the FAD N5 atom at the substrate C1 atom (Scheme 2b), generating a flavin−Gal*p* intermediate with transient release of UDP (Scheme 2c). Subsequent proposed steps also involving flavin−sugar intermediates include proton transfers, opening of the Gal*p* ring, and ring contraction to Gal*f* (Scheme 2c−f). Finally, the sugar−UDP bond is re-formed to generate UDP-Gal*f* (Scheme 2g,h).

Scheme 2. Mechanism of UGM

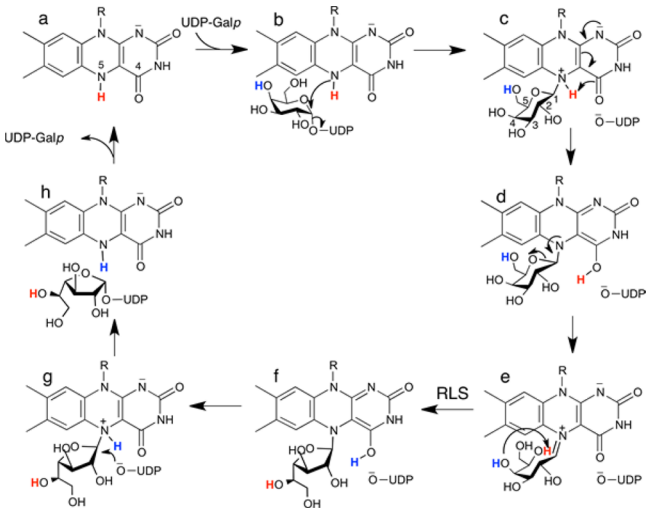

Covalent flavin−sugar intermediates are distinguishing features of this unusual flavoenzyme mechanism, and much effort has been spent in seeking evidence of them. Landmark studies by Kiessling's group using borohydride trapping and

Received: January 14, 2016
Revised: January 29, 2016
Published: February 2, 2016

DOI: 10.1021/acs.biochem.6b00035
Biochemistry 2016, 55, 833−836

tritium labeling of the substrate revealed the first evidence of the flavin−iminium intermediate (Scheme 2e).[10] Later studies by the same group confirmed the structural identity of this intermediate using nuclear magnetic resonance of the trapped species.[11] Since then, additional indirect evidence implicating flavin−sugar intermediates in the UGM reaction has been obtained.[8,12,13] However, despite more than a decade of research on the UGM reaction mechanism, direct structural evidence of a flavin−sugar adduct has remained elusive. Herein, we report the first crystal structure of a UGM having a covalent bond between the FAD and galactose.

The structure was determined using an active site mutant of *A. fumigatus* UGM (AfUGM) in which His63 is mutated to Ala (H63A). His63 is part of the conserved histidine loop, which has the sequence GGHVIF in AfUGM. All UGMs have Gly and His at positions 1 and 3 of the loop, respectively.[14] As described previously, the conformation of the His loop of AfUGM depends on the redox state of the flavin.[14] In the reduced (active) state, the carbonyl of Gly62 accepts a hydrogen bond from flavin N5, while the side chain of His63 forms a hydrogen bond with the 2′-OH of the FAD ribityl group. These protein−flavin interactions are thought be essential for maintaining the active conformation of UGM.[14−17]

Consistent with the universal conservation of the eponymous residue of the histidine loop, the catalytic properties of H63A are highly perturbed. H63A lacks catalytic activity. Although the flavin in the mutant enzyme can be reduced by sodium dithionite, reduced H63A is highly susceptible to oxidation by O_2 compared to the wild-type (wt) enzyme (Figure S1). Furthermore, reduction of the flavin in H63A by NADPH is very slow. The efficiency of NADPH reduction (k_{red}/K_D) is 114 M^{-1} s^{-1}, compared to 120000 M^{-1} s^{-1} for wt AfUGM (Figure S2). These results are consistent with our previous study showing that this mutation in *T. cruzi* UGM (H62A) decreased k_{cat} for the mutase reaction by >300-fold.[16]

We serendipitously discovered that H63A could be used to capture a covalent FAD−Gal*p* adduct *in crystallo*. Electron density maps from crystals of H63A that had been soaked simultaneously in sodium dithionite and UDP-Gal*p* prior to being flash-cooled in liquid nitrogen surprisingly showed features consistent with covalent modification of the FAD at the N5 atom (Figure 1A). The soaking time and reagent concentrations were optimized to maximize the occupancy of the apparent intermediate, which required X-ray diffraction analysis of approximately 14 crystals. The structure reported here has a crystallographic resolution of 2.3 Å and was obtained from a crystal soaked for 2 h in 80 mM dithionite and 100 mM UDP-Gal*p* prior to flash-cooling (Table S1).

AfUGM crystallizes with a tetramer in the asymmetric unit, and the electron density in chain A provides the clearest depiction of a reaction intermediate. The map shows a strong feature indicating that the FAD is covalently modified at its N5 atom (Figure 1A). Also, strong electron density is present for UDP bound in the expected location (Figure 1A). The maps clearly indicated that the active site flaps are closed, which is expected when UDP is bound.[14] The electron density for UDP is disconnected from that of the covalent modification when viewed at a level of 1.0σ for the refined $2F_o - F_c$ map or >2.5σ for the simulated annealing $F_o - F_c$ omit map (Figure 1A), indicating the presence of two distinct ligands rather than an intact sugar nucleotide. These electron density features could be satisfactorily interpreted as Gal*p* bound to FAD through a

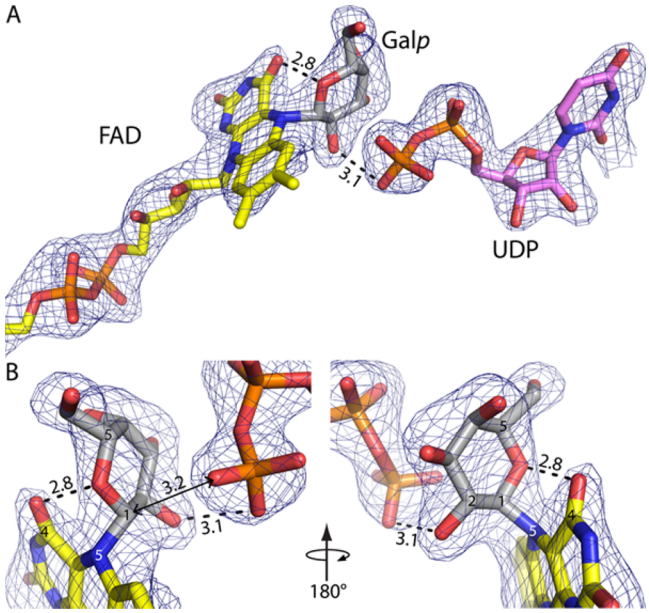

Figure 1. Electron density evidence of a covalent intermediate in the UGM reaction. The cage represents a simulated annealing $F_o - F_c$ omit map contoured at 3σ. Prior to map calculation, the FAD, Gal*p*, and UDP were deleted and simulated annealing refinement was performed. Distances are given in angstroms. (A) Overview of the ligands. FAD and Gal*p* are colored yellow and gray, respectively. UDP is colored pink. (B) Close-up views of the covalent adduct. This figure and others were made with PyMOL.[18]

Gal*p* C1−FAD N5 bond plus a detached UDP, which corresponds to intermediate c or d in Scheme 2.

The FAD−Gal*p* intermediate was refined using geometrical restraints obtained from quantum mechanics/molecular mechanics (QM/MM) calculations (Supporting Information).[19] The target Gal*p* C1−FAD N5 bond distance was 1.547 Å. This bond refined to 1.6 Å, indicating that the crystallographic data are consistent with the QM/MM calculations. The average *B* factors of the FAD and Gal*p* refined to 41.6 and 59.4 $Å^2$, respectively, with fixed occupancies of 1.0 (Table S1). After refinement, the shortest distance between C1 of Gal*p* and the O atoms of the UDP β-phosphate is 3.2 Å (Figure 1B), which is obviously outside of covalent bonding distance and consistent with rupture of the glycosidic bond during soaking.

Electron density in chain B was also modeled as intermediate c/d, but the density is not as strong as in chain A (Figure S3A). In chains C and D, the density suggests a possible mixture of covalent adducts without bound UDP (see Model Building Methods in the Supporting Information and Figure S3B,C). We thus focus the remaining discussion on the active site of chain A.

The trapped intermediate resembles the noncovalent complex of wt AfUGM with UDP-Galp (E−S complex), as one might expect for consecutive steps in a chemical mechanism. The conformation of UDP and its interactions with the enzyme are very similar to those of the E−S complex (Figure 2A). The Gal*p* of the intermediate likewise has a pose and protein environment similar to those in the E−S complex (Figure 2A). The O2 and O3 hydroxyls of the covalently bound Gal*p* form hydrogen bonds with Arg182. The Gal*p* O3 and O4 hydroxyls contact the side chain of Phe66 (3.4 Å). The Gal*p* O4 hydroxyl also forms a hydrogen bond with Asn207. The

DOI: 10.1021/acs.biochem.6b00035
Biochemistry 2016, 55, 833−836

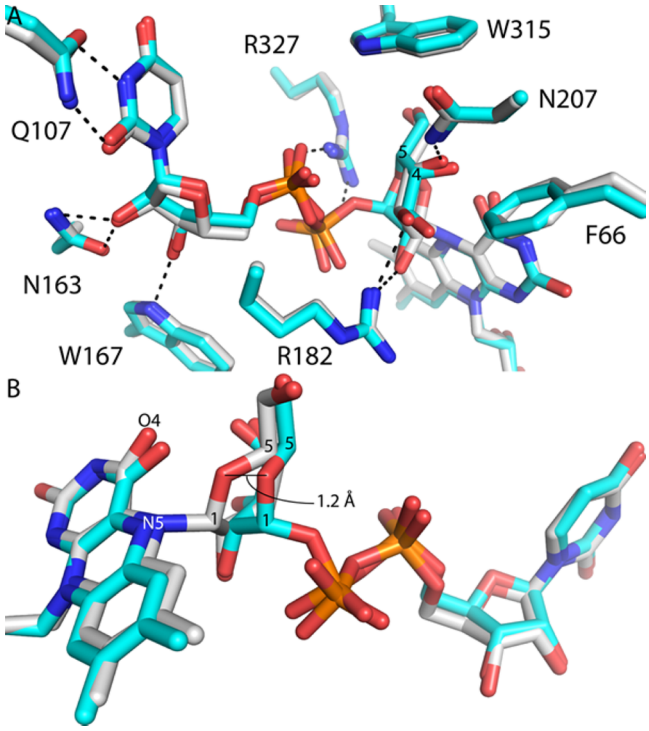

Figure 2. Comparison of the covalent intermediate in H63A (white) and the noncovalent E−S complex (cyan, Protein Data Bank entry 3UTH[15]). (A) Superposition of the two structures emphasizing the similarity of the UDP conformations and protein environment. The dashed lines indicate interaction distances of <3.1 Å. (B) Close-up showing how formation of the N5−C1 bond draws Gal*p* O5 closer to flavin O4.

Gal*p* O6 hydroxyl packs tightly between Trp315 (3.6 Å) and Arg327 (3.4 Å). All of these enzyme−sugar interactions are also seen in the E−S complex. The similarity of the H63A active structure to the genuine E−S complex implies that the species captured *in crystallo* is meaningful despite the use of a mutant enzyme.

A difference between the trapped intermediate and the E−S complex is that formation of the FAD N5−Gal*p* C1 bond draws O5 of Gal*p* 1.2 Å closer to the pyrimidine ring of the FAD isoalloxazine (Figure 2B). In the covalent intermediate, Gal*p* O5 is 2.8 Å from FAD O4 (Figure 1), compared to 3.3 Å in the E−S complex. The close approach of Gal*p* O5 and FAD O4 in the intermediate is consistent with a proposal from QM/MM calculations[20] that FAD O4 accepts a proton from FAD N5 and donates it to Gal*p* O5, facilitating ring opening and formation of the iminium ion (Scheme 2c−e).

Electron density for the histidine loop of the intermediate (Figure 3A) suggests a conformation similar to that of the reduced wt enzyme, except for one important aspect (Figure 3B). In reduced wt AfUGM (ligand-free or complexed with UDP-Gal*p*), the carbonyl of Gly62 accepts a hydrogen bond from flavin N5. Because N5 of the reduced FAD is an obligate hydrogen bond donor, the hydrogen bond with Gly62 is considered to be a key stabilizing interaction of the reduced enzyme.[14−17] Indeed, this hydrogen bond is found in other structures of reduced UGMs. In the H63A−Gal*p* adduct, however, Gly62 is rotated by ∼90° from the expected orientation so that it is not within hydrogen bonding distance of N5. This rotation appears to be necessary to avoid steric clash with Gal*p* O5. The rotation may also reflect a change in

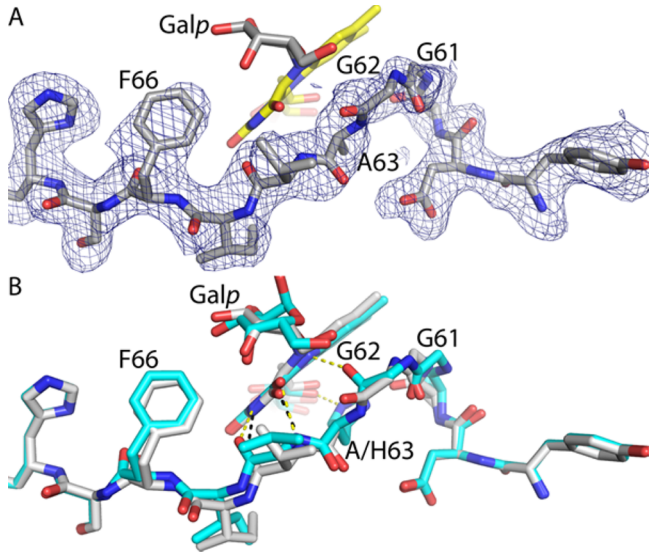

Figure 3. Conformation of the histidine loop. (A) Electron density for the histidine loop of H63A. The cage represents a simulated annealing $F_o - F_c$ omit map (2.25σ). Prior to map calculation, residues 58−68 were deleted and simulated annealing refinement was performed. The FAD is colored yellow. (B) Comparison of the loops of H63A (white) and the E−S complex (cyan, Protein Data Bank entry 3UTH). Black and yellow dashes indicate hydrogen bonds in H63A and the E−S complex, respectively.

the hydrogen bond capacity of FAD N5 in going from intermediate c to intermediate d in Scheme 2. In the latter state, N5 cannot donate a hydrogen bond, which could induce rotation of the Gly62 carbonyl, an obligate acceptor, away from N5. The orientation of Gly62 perhaps suggests that the trapped species is intermediate d rather than intermediate c, although it is impossible to distinguish between these species solely on the basis of the electron density at this resolution. Finally, it is also possible that mutation of His63 causes the atypical orientation of Gly62, and it is this structural perturbation that allowed us to capture the intermediate *in crystallo*.

In conclusion, we have determined the first crystal structure of a covalent intermediate in the UGM reaction. To the best of our knowledge, it is the first structure of a substrate-derived covalent intermediate for any noncanonical flavoenzyme. The structure confirms the role of FAD N5 as a nucleophile and supports the hypothesis that the proton destined for O5 of Gal*f* is transferred from FAD N5 via the FAD O4 carbonyl.

■ ASSOCIATED CONTENT

Supporting Information

The Supporting Information is available free of charge on the ACS Publications website at DOI: 10.1021/acs.biochem.6b00035.

Experimental methods, a table of X-ray data collection and refinement statistics, and supporting figures (PDF)

Accession Codes

Atomic coordinates and structure factor amplitudes have been deposited in the Protein Data Bank as entry 5HHF.

■ AUTHOR INFORMATION

Corresponding Authors

*E-mail: psobrado@vt.edu.
*E-mail: tannerjj@missouri.edu.

DOI: 10.1021/acs.biochem.6b00035
Biochemistry 2016, 55, 833−836

Author Contributions

R.M.-C. and Y.D. contributed equally to this work.

Funding

This research was supported by the National Institute of General Medical Sciences of the National Institutes of Health via Grant R01GM094469 and National Science Foundation Grant CHE-1506206 (to P.S. and J.J.T.).

Notes

The authors declare no competing financial interest.

■ ACKNOWLEDGMENTS

We thank Dr. Jay Nix for help with X-ray data collection and Dr. Isabel Da Fonseca for help with site-directed mutagenesis. Part of this research was performed at the Advanced Light Source, which is supported by the Director, Office of Science, Office of Basic Energy Sciences, of the U.S. Department of Energy under Contract DE-AC02-05CH11231.

■ REFERENCES

(1) Tefsen, B., Ram, A. F., van Die, I., and Routier, F. H. (2012) *Glycobiology 22*, 456−469.
(2) Pan, F., Jackson, M., Ma, Y., and McNeil, M. (2001) *J. Bacteriol. 183*, 3991−3998.
(3) Sassetti, C. M., Boyd, D. H., and Rubin, E. J. (2003) *Mol. Microbiol. 48*, 77−84.
(4) Schmalhorst, P. S., Krappmann, S., Vervecken, W., Rohde, M., Muller, M., Braus, G. H., Contreras, R., Braun, A., Bakker, H., and Routier, F. H. (2008) *Eukaryotic Cell 7*, 1268−1277.
(5) Kleczka, B., Lamerz, A. C., van Zandbergen, G., Wenzel, A., Gerardy-Schahn, R., Wiese, M., and Routier, F. H. (2007) *J. Biol. Chem. 282*, 10498−10505.
(6) Turner, C. W., Lima, M. F., and Villalta, F. (2002) *Biochem. Biophys. Res. Commun. 290*, 29−34.
(7) Beverley, S. M., Owens, K. L., Showalter, M., Griffith, C. L., Doering, T. L., Jones, V. C., and McNeil, M. R. (2005) *Eukaryotic Cell 4*, 1147−1154.
(8) Wesener, D. A., May, J. F., Huffman, E. M., and Kiessling, L. L. (2013) *Biochemistry 52*, 4391−4398.
(9) Novelli, J. F., Chaudhary, K., Canovas, J., Benner, J. S., Madinger, C. L., Kelly, P., Hodgkin, J., and Carlow, C. K. (2009) *Dev. Biol. 335*, 340−355.
(10) Soltero-Higgin, M., Carlson, E. E., Gruber, T. D., and Kiessling, L. L. (2004) *Nat. Struct. Mol. Biol. 11*, 539−543.
(11) Gruber, T. D., Westler, W. M., Kiessling, L. L., and Forest, K. T. (2009) *Biochemistry 48*, 9171−9173.
(12) Sun, H. G., Ruszczycky, M. W., Chang, W. C., Thibodeaux, C. J., and Liu, H. W. (2012) *J. Biol. Chem. 287*, 4602−4608.
(13) Oppenheimer, M., Valenciano, A. L., Kizjakina, K., Qi, J., and Sobrado, P. (2012) *PLoS One 7*, e32918.
(14) Tanner, J. J., Boechi, L., Andrew McCammon, J., and Sobrado, P. (2014) *Arch. Biochem. Biophys. 544*, 128−141.
(15) Dhatwalia, R., Singh, H., Oppenheimer, M., Karr, D. B., Nix, J. C., Sobrado, P., and Tanner, J. J. (2012) *J. Biol. Chem. 287*, 9041−9051.
(16) Dhatwalia, R., Singh, H., Oppenheimer, M., Sobrado, P., and Tanner, J. J. (2012) *Biochemistry 51*, 4968−4979.
(17) Dhatwalia, R., Singh, H., Solano, L. M., Oppenheimer, M., Robinson, R. M., Ellerbrock, J. F., Sobrado, P., and Tanner, J. J. (2012) *J. Am. Chem. Soc. 134*, 18132−18138.
(18) DeLano, W. L. (2012) *The PyMOL Molecular Graphics System*, version 1.8, Schrödinger, LLC, Portland, OR.
(19) Pierdominici-Sottile, G., Cossio Perez, R., Galindo, J. F., and Palma, J. (2014) *PLoS One 9*, e109559.
(20) Huang, W., and Gauld, J. W. (2012) *J. Phys. Chem. B 116*, 14040−14050.

DOI: 10.1021/acs.biochem.6b00035
Biochemistry 2016, 55, 833−836

Supporting Information

In Crystallo Capture of a Covalent Intermediate in the UDP-Galactopyranose Mutase Reaction

Ritcha Mehra-Chaudhary,[†,^] Yumin Dai,[§,^] Pablo Sobrado,[§,*] and John J. Tanner[‡,*]

[†]Structural Biology Core, University of Missouri-Columbia, Columbia, MO 65211, USA; [§]Department of Biochemistry and Center for Drug Discovery, Virginia Tech, Blacksburg, VA 24061, USA; [‡]Departments of Biochemistry and Chemistry, University of Missouri-Columbia, Columbia, MO 65211, USA. [^]These authors contributed equally to this work.

Corresponding authors
[*]Department of Biochemistry, Virginia Tech, Blacksburg, VA 24061. Phone (540) 231-9485. Fax (540) 231-9070. E-mail: psobrado@vt.edu.
Department of Biochemistry, University of Missouri-Columbia, Columbia, MO 65211. Phone: (573) 884-1280. E-mail: tannerjj@missouri.edu.

Table of Contents

EXPERIMENTAL PROCEDURES

Site-Directed Mutagenesis and Protein Production. Protein expression was performed using autoinduction media and following procedures developed previously for wild-type *Aspergillus fumigatus* UDP-galactopyranose mutase (AfUGM) [1].

Kinetics Measurements. Conversion of UDP-Gal*f* to UDP-Gal*p* was monitored by HPLC as previously described [1]. Even at the highest concentration of H63A (10 μM) and UDP-Gal*f* (100 mM) no activity was observed.

The reaction of H63A with NADPH was monitored in a SX-20 stopped-flow spectrophotometer (Applied Photophysics, Leatherhead, UK) housed in an anaerobic glove box (Coy, Grass Lake, MI) following methods previously described (*2*). H63A (50 μM after mixing) was mixed with various concentrations of NADPH (0.05-1.0 mM after mixing) under anaerobic conditions. The changes in absorbance (at 452 nm) were fit to a single exponential decay equation (eq. 1) to obtain the rate constant (k_{obs}) at each substrate concentration. Kinetic parameters for the reduction of the enzyme as a function of NADPH were obtained by fitting the k_{obs} values to eq. 2, where k_{red} is the rate constant for flavin reduction, and K_D is the dissociation constant for NADPH.

$$v = c + ae^{-(k_{obs}t)} \quad (1)$$

$$k_{obs} = \frac{k_{red}[NADPH]}{K_D + [NADPH]} \quad (2)$$

In order to measure the reactivity of wild-type AfUGM and H63A with oxygen, the enzymes were first reduced by reacting 100 μM enzyme with 20 mM dithionite for 20 min under anaerobic conditions (in the glove box). The solution was passed through a desalting column to separate the enzymes from excess dithionite. The resulting reduced enzyme was mixing with

various concentrations of oxygen (0.2, 0.4, 0.6 mM) in the stopped-flow spectrophotometer. Flavin oxidation was monitored at 452 nm and the changes in absorbance were fit to eq. 3, which describes a single exponential rise.

$$v = c + a(1 - e^{-(k \times t)}) \qquad (3)$$

Crystallization. For crystallography, the His63Ala mutation was created in a plasmid encoding the AfUGM double surface mutant K344A/K345A. As described previously, mutation of Lys344 and Lys345 to Ala facilitates crystallization of a high resolution hexagonal crystal form and does not affect activity [1]. For simplicity, we will refer to the triple mutant H63A/K344A/K345A as H63A.

Crystals of oxidized H63A were grown using ammonium sulfate as the precipitant as described for the wild-type enzyme and other AfUGM mutants [1,2]. Briefly, the crystallization was carried out in Cryschem sitting drop trays at 20 °C. The 500 μL reservoir solution contained 1.6 M ammonium sulfate and 0.1 M sodium acetate at pH 4.5. The drops were set up by mixing 1.5 μL of protein at 22 mg/mL with an equal volume of reservoir solution. Fresh Tris(3-hydroxypropyl)phosphine (THP, 1 mM) was added to the protein just prior to setting up the trays. To speed up crystallization, microseeding was carried out with crushed wild type AfUGM seeds. As with wild-type AfUGM, the space group of H63A crystals is $P6_522$ with unit cell lengths of a = 218 Å and c = 320 Å and one tetramer in the asymmetric unit.

Crystal Soaking. A substrate-derived covalent intermediate was captured *in crystallo* by soaking at room temperature as follows. The sitting drop containing suitable crystals was opened and 25 μL of the reservoir solution was added to the drop. This solution was slowly exchanged into a series of cryobuffers containing 1.8 M ammonium sulfate and 0.1 M sodium acetate at pH 4.5 with increasing concentrations of the cryoprotectant meso-erythritol to a final

meso-erythritol concentration of 35%. The cryoprotected crystals were reduced by incubating with the final cryobuffer supplemented with 80 mM sodium dithionite (reducing cryobuffer). Reduction was evident from the bleaching of the yellow color of the crystals. Next, the crystals were soaked for 2 hours in the reducing cryobuffer supplemented with 100 mM UDP-galactopyranose (UDP-Gal*p*). The crystals were then picked up with nylon loops and flash-cooled in liquid N_2 and stored until data collection.

X-ray Diffraction Data Collection and Processing. X-ray diffraction data were collected at beamline 4.2.2 of the Advanced Light Source using a CMOS-based Taurus-1 detector in shutterless mode. The data set used for refinement was collected with a detector distance of 270 mm and consisted of 900 frames covering 180° with a total exposure time of 360 s. The data were integrated and scaled with XDS [3]. Intensities were merged and converted to amplitudes with Aimless [4]. Data processing statistics are listed in Table S1.

Refinement. Refinement using PHENIX [5] was initiated from the protein coordinates (histidine loop removed) of reduced AfUGM complexed with UDP-Gal*p* (PDB code 3UTH). The first round of refinement used rigid body refinement and simulated annealing. The B-factor model consisted of one TLS group per protein chain and an isotropic B-factor for each non-hydrogen atom. Non-crystallographic restraints were used during refinement. All atoms have occupancy of 1.0. Refinement statistics are listed in Table S1.

Restraint files needed for crystallographic refinement of the covalently-modified flavin were generated with PHENIX eLBOW [6] using the coordinates of reaction intermediates predicted from quantum mechanics-molecular mechanics (QM/MM) calculations. These coordinate files were obtained from the Supporting Information of [7]. In PHENIX eLBOW, geometry optimization was disabled and the input coordinates were selected to be the "final geometry".

These options ensured that the resulting target bond and angle restraints corresponded to those of the QM/MM model. Otherwise, the default optimization algorithm of PHENIX eLBOW, which uses a much lower level of theory than in [7], severely distorted the geometry of the intermediate.

Model Building. The covalent intermediate bound to the flavin in chains A and B of the tetramer in the asymmetric unit was refined using restraints calculated from a QM/MM model of intermediate c in Scheme 2 (corresponds to Figure 2b of [7]). We note that at 2.3 Å resolution it is difficult to distinguish between intermediates c and d in Scheme 2, since they differ only in the position of a proton. Nevertheless, refinement using restraints calculated from a QM/MM model of intermediate d (Scheme 2) was unsatisfactory because the Gal*p* ring moved out of density.

The electron density features in the active sites of chains C and D of the tetramer are not as readily interpretable as in chain A. We note that differential binding of ligands from soaking this crystal form is common; typically, active site ligands bind with high occupancy to chains A and B but not to chains C and D [1,2]. In chains C and D of reduced H63A soaked with UDP-Gal*p*, electron density for UDP is absent, however; the maps strongly suggest covalent modification of the FAD at the N5 position (Figures S3B, S3C). The active site flaps are clearly open in chains C and D, which is consistent with the absence of UDP. For testing purposes, the modified flavin was modeled with a bound cyclic Gal*p* (Scheme 2c/d), linear sugar (Scheme 2e) or cyclic Gal*f* (Scheme 2f/g). Refinement as FAD-Gal*p* (Scheme 2c) yielded the best result in terms of fit to the refined $2F_o$-F_c electron density and steric clashes with surrounding residues, however; the model-map correspondence was not as satisfactory as in chains A and B (Figures S3B, S3C). We also tried modeling an N5-sulfite adduct, which can appear in dithionite-reduced flavoenzyme crystals [8,9], but the results were less satisfactory than the cyclic sugar models.

Our interpretation of the electron density in chains C and D is that nucleophilic attack occurred, and the displaced UDP diffused out of the active site because the active site flaps are locked in the open state by crystal packing interactions. The electron density likely represents an FAD-Gal*p* adduct with conformational disorder and/or a mixture of FAD-sugar intermediates. Thus, although the flavin is covalently modified in chains C and D, we could not definitively account for the density using a single model of any of the expected intermediates in the reaction. Therefore, the flavin in chains C and D was modeled as an unmodified, reduced FAD.

Table S1. Data Collection and Refinement Statistics[a]

Beamline	ALS 4.2.2
Space group	$P6_522$
Unit cell parameters (Å)	a =217.5, c =319.8
Wavelength	1.0000
Resolution (Å)	61.61-2.30 (2.34-2.30)
Observations	4132787
Unique reflections	196082
$R_{merge}(I)$	0.201 (1.45)
$R_{meas}(I)$	0.206 (1.49)
$R_{pim}(I)$	0.045 (0.329)
Mean $CC_{1/2}$	0.998 (0.814)
Mean I/σ	15.1 (2.5)
Completeness (%)	100.0 (100.0)
Multiplicity	21.1 (20.5)
No. of protein residues	2015
No. of atoms	
Protein	15448
FAD	212
Gal*p*	22
UDP	50
Water	740
R_{cryst}	0.1845 (0.2704)
R_{free}[b]	0.2134 (0.3520)
rmsd bond lengths (Å)	0.007
rmsd bond angles (°)	0.945
Ramachandran plot[c]	
Favored/Allowed (%)	97.80/2.15
Outliers (%)	0.05
Clashscore (percentile)[c]	2.18 (100th percentile)
MolProbity score (percentile)[c]	1.06 (100th percentile)
Average B (Å^2)	
Protein	39.3
FAD[d]	41.6, 38.9, 47.2, 51.7
Gal*p*[d]	59.4, 70.5, N/A, N/A
UDP[d]	50.7, 55.2, N/A, N/A
Water	38.8
Coordinate error (Å)[e]	0.25
PDB code	5HHF

[a]Values for the outer resolution shell of data are given in parenthesis. [b]Random 2% test set. [c]Generated with MolProbity [10]. [d]Values for the four chains of the tetramer in the asymmetric unit are listed as A, B, C, D. [e]Maximum likelihood-based coordinate error estimate from PHENIX refine.

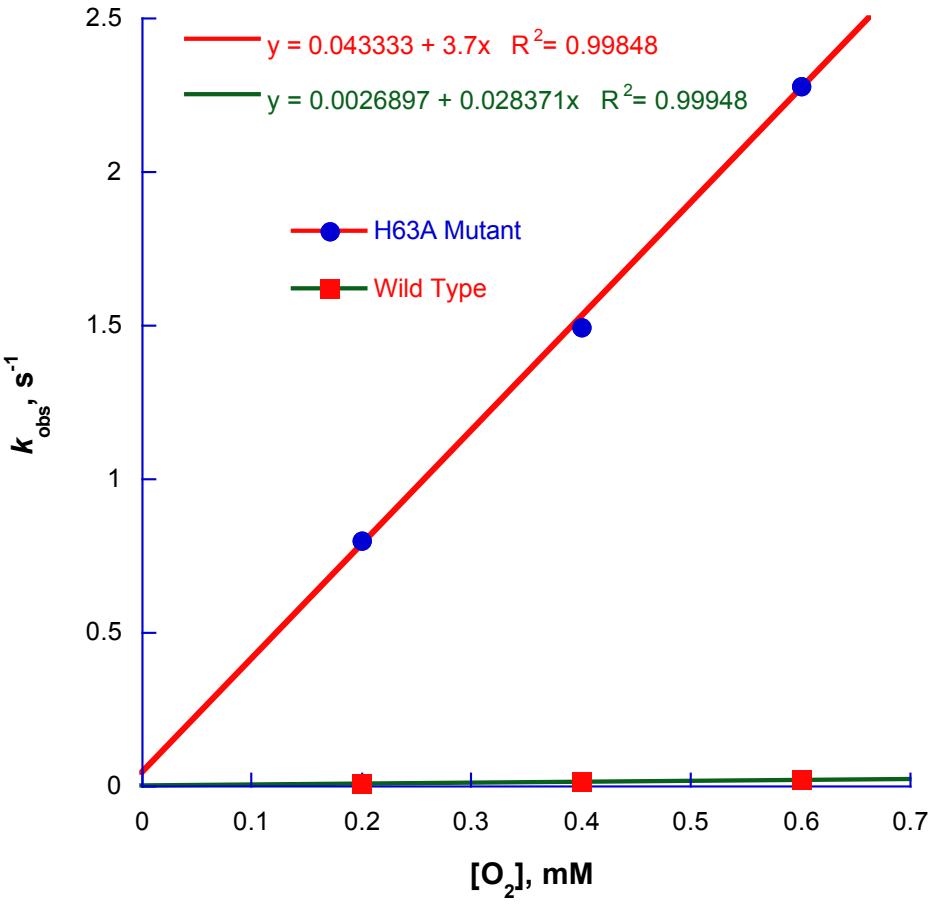

Figure S1. Susceptibility of reduced H63A to reaction with O_2. The first-order rate constants for the reaction of O_2 with dithionite-reduced H63A and wild-type AfUGM are plotted as functions of the O_2 concentration. Note that the wild-type enzyme resists oxidation under these conditions.

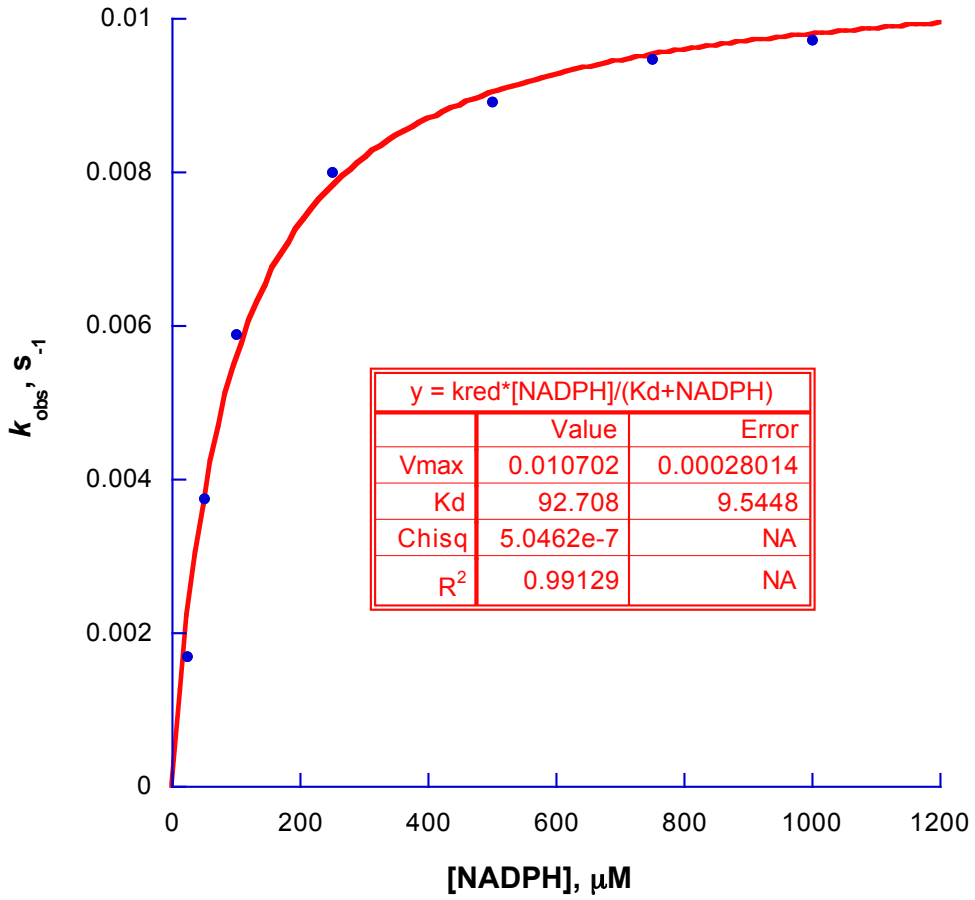

Figure S2. Kinetics of the reduction of H63A by NADPH. The first-order rate constant for the reaction of NADPH with H63A is plotted as function of the NADPH concentration. The inset shows the kinetic constants obtained from fitting the data to eq. 2 (k_{red}= 0.0106 ± 0.0003 s^{-1} and K_D = 92.7 ± 9.5 μM). For comparison, the values for the wild-type enzyme are k_{red} = 3 s^{-1} and K_D = 25 μM.

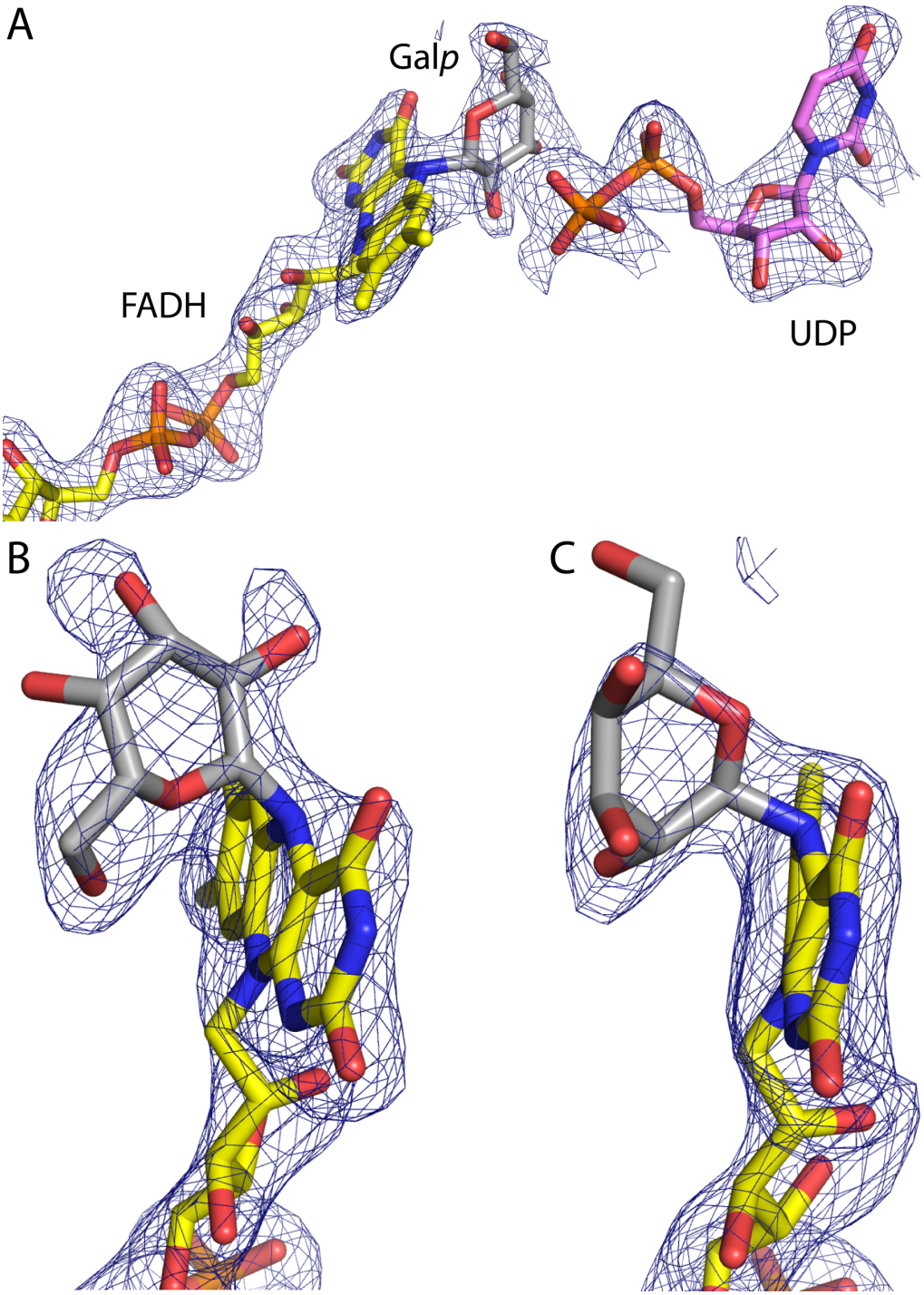

Figure S3. Electron density for ligands bound to chains B, C, and D of the tetramer. The cages represent a simulated annealing F_o - F_c omit map contoured at 3.0 σ. Prior to calculation of the map, the ligands were deleted and simulated annealing refinement was performed in PHENIX. (A) The modified flavin and UDP in chain B. (B) The modified flavin in chain C. Gal*p* is not included in the coordinate file that has been deposited in the PDB (code 5HHF), but is shown here to guide the eye. (C) The modified flavin in chain D. Gal*p* is not included in the coordinate file that has been deposited in the PDB (code 5HHF), but is shown here to guide the eye.

REFERENCES

[1] R. Dhatwalia, H. Singh, M. Oppenheimer, D.B. Karr, J.C. Nix, P. Sobrado, J.J. Tanner, Crystal structures and small-angle X-ray scattering analysis of UDP-galactopyranose mutase from the pathogenic fungus Aspergillus fumigatus, J. Biol. Chem. 287 (2012) 9041–9051.

[2] I. Da Fonseca, I.A. Qureshi, R. Mehra-Chaudhary, K. Kizjakina, J.J. Tanner, P. Sobrado, Contributions of Unique Active Site Residues of Eukaryotic UDP-Galactopyranose Mutases to Substrate Recognition and Active Site Dynamics, Biochemistry 53 (2014) 7794-7804.

[3] W. Kabsch, XDS, Acta Crystallogr. D Biol. Crystallogr. 66 (2010) 125-132.

[4] P.R. Evans, G.N. Murshudov, How good are my data and what is the resolution?, Acta Cryst. D69 (2013) 1204-1214.

[5] P.V. Afonine, R.W. Grosse-Kunstleve, N. Echols, J.J. Headd, N.W. Moriarty, M. Mustyakimov, T.C. Terwilliger, A. Urzhumtsev, P.H. Zwart, P.D. Adams, Towards automated crystallographic structure refinement with phenix.refine, Acta Crystallogr. D Biol .Crystallogr. 68 (2012) 352-367.

[6] N.W. Moriarty, R.W. Grosse-Kunstleve, P.D. Adams, electronic Ligand Builder and Optimization Workbench (eLBOW): a tool for ligand coordinate and restraint generation, Acta Crystallogr. D Biol. Crystallogr. 65 (2009) 1074-1080.

[7] G. Pierdominici-Sottile, R. Cossio Perez, J.F. Galindo, J. Palma, QM/MM molecular dynamics study of the galactopyranose --> galactofuranose reaction catalysed by Trypanosoma cruzi UDP-galactopyranose mutase, PLoS One 9 (2014) e109559.

[8] T.C. Tan, W. Pitsawong, T. Wongnate, O. Spadiut, D. Haltrich, P. Chaiyen, C. Divne, H-bonding and positive charge at the N5/O4 locus are critical for covalent flavin attachment in trametes pyranose 2-oxidase, J Mol Biol 402 (2010) 578-594.

[9] E. Golden, A. Karton, A. Vrielink, High-resolution structures of cholesterol oxidase in the reduced state provide insights into redox stabilization, Acta Crystallogr D Biol Crystallogr 70 (2014) 3155-3166.

[10] V.B. Chen, W.B. Arendall, 3rd, J.J. Headd, D.A. Keedy, R.M. Immormino, G.J. Kapral, L.W. Murray, J.S. Richardson, D.C. Richardson, MolProbity: all-atom structure validation for macromolecular crystallography, Acta Crystallogr. D Biol. Crystallogr. D66 (2010) 12-21.